Title	Infrared spectroscopy study of a poly-silicon film for optimizing the boron-implanting dose
Author(s)	Tuohiniemi, Mikko; Blomberg, Martti; Gao, Feng
Citation	Journal of Microelectromechanical Systems. IEEE. Vol. 22 (2013) No: 5, Pages 1207 - 1212
Date	2013
URL	http://dx.doi.org/10.1109/JMEMS.2013.2262580
Rights	Post-print version of the article.

Infrared spectroscopy study of a poly-silicon film for optimizing the boron-implanting dose

Mikko Tuohiniemi, Martti Blomberg, and Feng Gao

***Abstract*— An experiment was carried out for recording the infrared transmission between 3 and 16 µm for a free-standing poly-Si thin film as a function of the boron-ion implanting. The optical constants were extracted in order to optimize the post-deposition implanting of the membranes in a surface micro-machined Fabry-Perot interferometer for the thermal infrared. The free-carrier concentration must not degrade the refractive index *n* significantly since a high and constant value over the application wavelength range is desired. Moreover, an increase in the extinction coefficient *k* is detrimental for the interferometer performance. On the other hand, poly-silicon electrical conductivity must be doped high enough to avoid static charging and to prevent any layout-dependent distribution of the applied control voltage.**

We applied the variable-angle transmission spectrometry for recording the data of suspended poly-silicon membranes, doped with different levels of implanting dose. The Drude-model dispersion formula was exploited for extracting the optical constants $n(\lambda)$ and $k(\lambda)$. The optical constants are presented as a function of the dopant concentration and of the electrical resistivity.

***Index Terms*— Polysilicon, optical constants, boron, implanting**

I. Introduction

OUR objective is to resolve the thermal infrared (TIR) transmission of a free-standing poly-crystalline Si (poly-Si) film as a function of the boron-implanting dose. The vast literature data of the optical and electrical properties of the single-crystalline (sc) bulk Si [1],[2] provides a basis for concept design also for the surface micro-machined opto-electro-mechanical systems (MOEMS) of poly-Si. Numerical studies on the Si IR optical response have been published since the early era of electronic computers [3]. Experimental IR data of surface-implanted sc-Si has also been available for decades [4],[5]. Experiments on the Si thin films optical properties at the visible (VIS) and the near-IR (NIR) spectra have been published especially for amorphous hydrogenated Si (*a*- or *α*- Si:H), with the application in solar cells [6]-[8], but also for poly-Si [7]-[10].

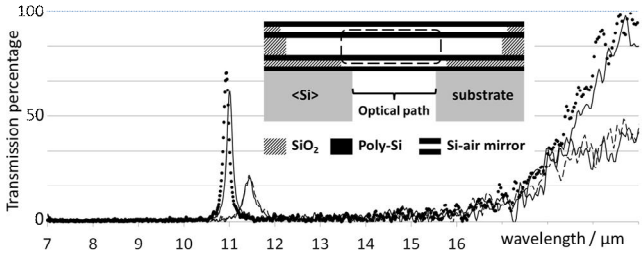

Fig. 1. MEMS TIR-FPI transmission peak with low (tall peaks) and too high (shallow peaks) implanting dose in the mirrors at the optical path. The data of two samples for each case is displayed. The peak spectral location does not depend on the implanting but is chosen separated for clarity. The inset illustrates a schematic cross section of the device. Dash line encircles the poly-Si films implanted area at the optical path.

Our application of the poly-Si film is a distributed Bragg reflector [11] of a MOEMS Fabry-Perot interferometer (FPI) [12], tuneable over the TIR wavelengths 7 µm < λ < 11 µm. A pair of sacrificially released free-standing poly-Si membranes forms a Si-air Bragg mirror [13], as schematically illustrated in Fig. 1. Silicon at TIR exhibits low losses and, the refractive-index *n* provides an excellent contrast with air or vacuum. Other established MEMS materials do not match these specifications.

In order to avoid static charging and to enable well-defined electrostatic actuation of the FPI adjustable mirror, certain poly-Si films must be tuned for sufficient electrical conductivity by means of the post-deposition ion implanting. However, at the optical path of the device, the doping-induced free-carrier concentration must not significantly affect the poly-Si optical constants.

The potential shifting of *n* is downwards. The contrast between the indices of the mirror air and the poly-Si layers would also go down and the mirror reflectivity degrades. Another, equally fatal, consequence of a too high carrier density is the increased absorption. At TIR region, high-resistivity silicon is practically lossless with the extinction coefficient $k < 10^{-3}$ whereas, $k > 10^{-2}$ degrades the transmission below an acceptable level. The design and the performance of the TIR-FPI are published elsewhere [14] but here, for reference, we show in Fig. 1 how a non-optimal implanting level in the poly-Si film degrades the FPI

Manuscript received October 9, 2012. This work was fully funded by the VTT internal research budget.

M. Tuohiniemi and F. Gao are with the VTT Technical Research Centre of Finland, Tietotie 3, Espoo, P.O. Box 1000, FI-02044 VTT, Finland (phone: +358-20-7224885; e-mail: mikko.tuohiniemi@vtt.fi).

M. Blomberg is with VTT Memsfab Ltd, PO Box 1000, FI-02044 VTT, Finland

transmission properties.

The design optimization of the FPI assumes data on the poly-Si film optical properties at TIR as a function of the implanting. The earlier data for sc-Si was not considered safe to rely on. For the best validity of the data, a test that imitates the poly-Si film function in the device is suggested. We concluded to carry out a variable-angle transmission spectroscopy experiment for free-standing suspended poly-Si films. The transmission spectrum reflects the same interference, between the film Si-air interfaces, that underlies the transmission of the complete FPI device in Fig.1. Even though the raw data already indicates the sought answers of proper implanting doses, we interpreted the data into the optical constants by model fitting. Finally, the film resistivity ρ was also measured in order to present the $n(\rho)$ and $k(\rho)$ for this same poly-Si material.

Dedicated tools for recording the thin-film material optical constants at TIR are not commonly available. The commercial instruments for shorter wavelengths up to NIR are typically reflectometers or ellipsometers [15],[16] but a self-made setup, based on a general-purpose Fourier-transform IR (FT-IR) spectrometer, suggests to avoid reflection measurements. The measurement setup for transmission eliminates the problems of aiming the signal beam at the detector while turning the angle of incidence. Complementary reflection data was considered unnecessary also for the reason that the signal scattering is negligible with the film roughness, thickness, and grain size well below the wavelength.

TABLE I
SAMPLE WAFERS IMPLANTING PARAMETERS

Wafer	Area dose / cm^{-2}	Volume dose / cm^{-3}	Annealing T / °C
1	5×10^{12}	7.8×10^{16}	850
2	1×10^{13}	1.6×10^{17}	850
3	2×10^{13}	3.1×10^{17}	850
4	5×10^{13}	7.8×10^{17}	850
5	1×10^{14}	1.6×10^{18}	850
6	5×10^{14}	7.7×10^{18}	850
7	1×10^{15}	1.5×10^{19}	850
8	5×10^{15}	7.7×10^{19}	850
9	2×10^{13}	3.1×10^{17}	700
10	2×10^{13}	3.1×10^{17}	1000
11	5×10^{14}	7.8×10^{18}	700
12	5×10^{14}	7.7×10^{18}	1000

Note that the doses per volume are computed based on the film thicknesses gained through fitting the transmission data with the Drude-model dispersion relation. This is why samples 6, 11 and 12 values are not identical even though the area doses are.

II. EXPERIMENT

A. Sample Preparation

The sample-wafers were prepared to provide free-standing poly-Si thin films with different doses of B^+ implanting for p-type doping. The substrate is deep etched open such that the transmission is purely measured through the poly-Si film alone. Care must be taken in the process design to ensure a wide enough film survives the manufacturing. Since a practical measurement setup requires millimetres wide membranes for a reasonable signal level, and the application dictated ca. 650 nm film thickness, the dimensions feature an aspect ratio more than 6000. The process flow is illustrated in Fig. 2 and sample parameters are tabulated in Table 1.

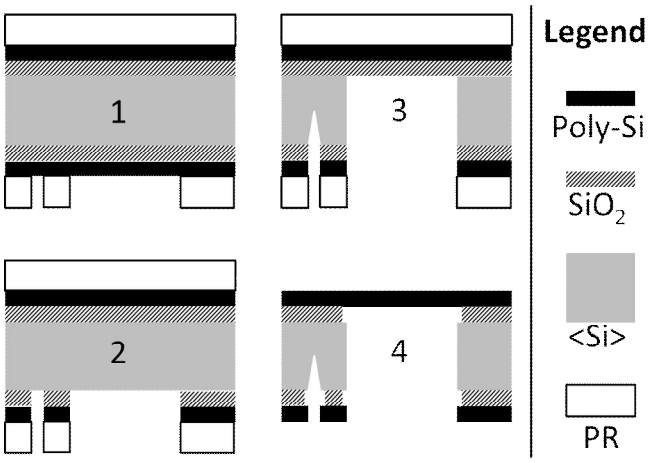

Fig. 2. Sample-preparation process flow. 1: SiO2, poly-Si films and lithography, 2: films plasma etching, 3: substrate DRIE, 4: PR-strip and HF-vapour SiO2 removal.

The samples had a 500 nm LPCVD SiO_2 deposited on the substrate for both the implanting isolation and for the later deep-etching stopping layer. A film of amorphous Si was deposited (Centrotherm tube, temperature T=580°C, silane flow 116 sccm, p=300 mTorr) and boron-ion implanted (V=50 keV, I=250µA, no tilt). Next, high-T annealing for 2 hours brings the film into poly-crystalline form, into proper tensile stress, and activates the B^+-ions into acceptor impurities. The annealing T was varied with samples 9-12 since, in the MEMS FPI, that is the method to adjust the films stress.

A layout of 4-mm-diameter circular openings was patterned and plasma etched through the poly-Si and SiO_2 layers. The pattern was opened through the substrate by means of the anisotropic deep reactive ion etching (DRIE, Aviza Omega i2L). The aspect-ratio dependent etching provided snap-off grooves that terminated at near the half depth of the substrate. Now the membrane was a free-standing stack of SiO_2, poly-Si, and protective photo resist (PR) that faces the etcher chuck. The Poly-Si layer is in a tensile stress determined by the annealing T. The PR layer is in tensile as well and, the SiO_2 in compressive stress. The net stress of the stack varied such that the samples with the lowest poly-Si annealing T (see table 1) were spun straight whereas, those of the highest T, appeared buckled due to net compressive stress. The last processing steps were PR

stripping in O_2 plasma and, finally, the SiO_2 removal in an anhydrous hydro-fluoric acid (HF) vapour etcher (Primaxx MEMS-CET). The highest-*T* annealed poly-Si films returned spun straight only after the SiO_2 removal. Yield losses up to 30 % were suffered with the samples of the highest poly-Si stress. Those most warped due to the buckling after the DRIE step finally resulted the best yield. If the temperature effects were not of interest, over 900°C annealing would have been preferred for all samples.

B. Measurements and Data Processing

IR Transmission

Optical transmission data over the TIR wavelengths 3 µm – 16 µm was recorded using a FT-IR spectrometer (Bruker Vector22) with a wavenumber resolution set to 20 cm^{-1}. The data points were saved at 7.7 cm^{-1} steps which translates to 7 nm – 200 nm or relatively 0.2 % - 1.2 % in wavelengths. As shown in Fig. 3, two external fixed apertures at both sides of the sample were pre-aligned to screen the signal so that, laterally on the sample, only the area within the free-standing membrane contributed to the data. The variable-angle measurement was done at incident angles of 0, 15, 30, and 45 degrees. The source-side aperture was tilted at a 20° angle, as a compromise between 0° and 45°, for enabling a shorter distance to the sample. The sample was mounted on an X-Z manipulator for the centring by means of signal-maximum finding after every rotation around the Z axis.

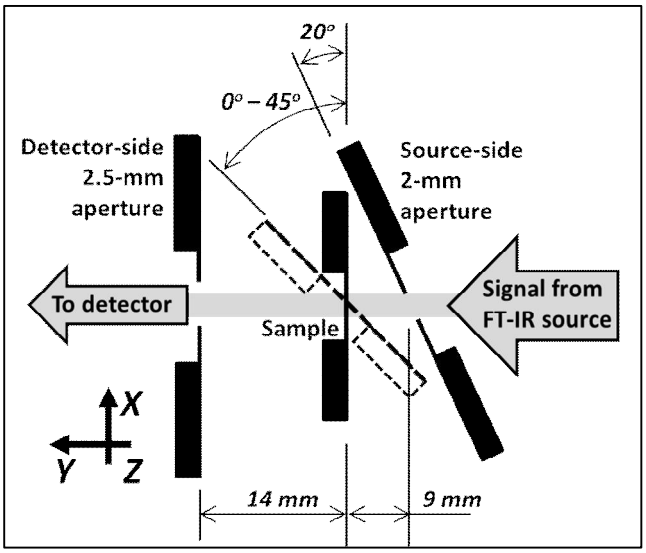

Fig. 3. The setup in the FT-IR chamber. Note how sample rotation determines the apertures location and adds the necessary sample-membrane diameter.

The sample chamber was purged with dry air for ca. 10 minutes after opened for adjusting the incident angle and for centring the sample. A wide H_2O absorption band at 5.5 – 7.5 µm was eliminated but a narrow CO_2 absorption at 4.2 µm was simply accepted uncontrolled and finally excluded from the data. For each sample mounting, a new background spectrum was recorded. The background was confirmed after completing the sample measurement at each 4 incident angles. A maximum shift of 0.3 % was accepted for the background signal level during the measurements of one sample.

$$n^2(\lambda) - k^2(\lambda) = A_0 \frac{A_1 A_2^2 \lambda^2}{\lambda^2 + A_2^2} \quad (1)$$

$$2\,n(\lambda)k(\lambda) = \frac{A_1 A_2^2 \lambda^3}{\lambda^2 + A_2^2} \quad (2)$$

The data was fitted in a model using the Drude-model [17] dispersion relation given in (1)-(2), where λ is the wavelength, n is the refractive index, k is the extinction coefficient and, $A_{1,2,3}$ are model-fitting parameters. A commercial software (TF-Calc ver. 3.5.6, Software-Spectra Inc.) was applied for extracting the optical constants $n(\lambda)$ and $k(\lambda)$ over the spectrum. Since the interference between the Si-air interfaces contributes the film data with information of the film thickness, it was left as an open parameter in the fitting. The wafer-to-wafer variation of +/- 0.7 % around the thickness average 646 nm was compared against a scanning electron microscope (SEM, Leo Supra 35) study of each individual sample, which resulted in 653 nm +/- 0.9 %. The low variation suggests that the film-deposition and the thickness determination, as error sources, are insignificant in extracting the electrical resistivity and the optical constants.

Electrical Resistivity

The poly-Si film electrical resistivity was extracted from bipolar current-voltage (IV) scans on resistance-bridge structures and from the film-thickness data mentioned above. Sheet resistances were not studied.

Lightly-doped poly-Si does not form an Ohmic contact but a Schottky-diode with the Al probe-contact pads. The IV-relation for a given test structure was saved at a voltage clearly above the back-to-back diode pair break-down voltage, which implied near 10 V for the lowest-dose (< 10^{14} cm^{-2}) implanted samples. Otherwise identical poly-Si bridges that only differ in length were measured at the same current. This differential method guarantees the same voltage drop at the non-Ohmic pad contacts. The difference is only due to the bridge length and the film resistivity is readily extracted.

The 10 V for the low-dose samples had to be decreased down to 1 V for the high-dose samples. Otherwise, their more Ohmic-behaving pad contacts allow enough current for heating the poly-Si bridge. The resistive power is $P=R*I^2$, where R is the computed differential resistance. For P > 100 nW, heating was revealed by observing that a quick repetition or a longer integration time affected the result.

III. RESULTS

The primary result was the transmission spectrum over the wavelength range as a function of the implanting dose, film annealing *T*, and of the angle of incidence. A visual inspection of the curves in Fig. 4 shows how samples 6-8 deviate in the transmission properties. The implanting doses above 10^{14} cm^{-2} must be rejected in the TIR-FPI design.

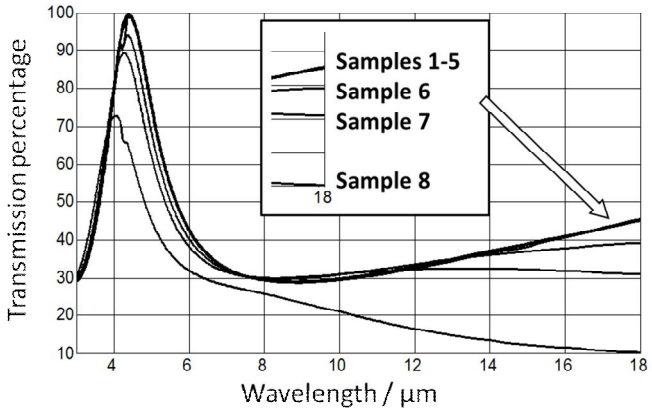

Fig. 4. FT-IR transmission spectra. Only the 15-degree incident angle data is shown as an example.

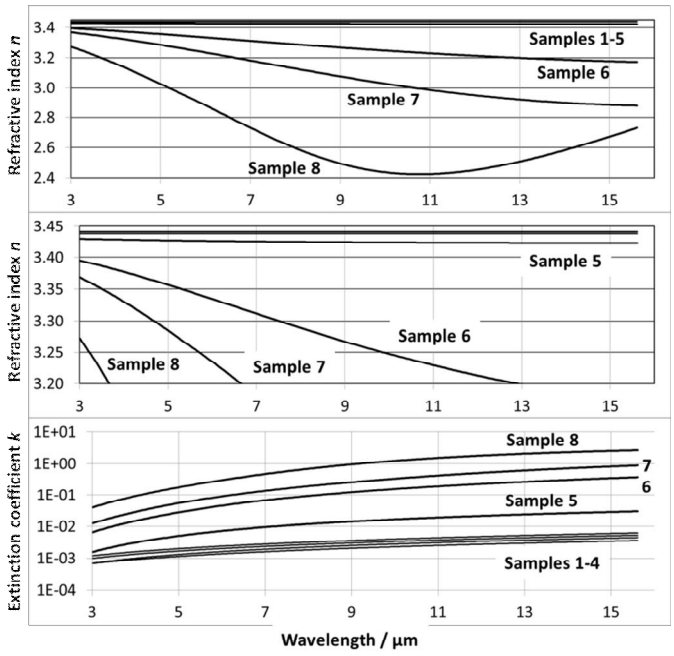

Fig. 5. The Drude-model fit results of *n* and *k*. The graph in the middle magnifies the region of the n-scale of the lightly-doped samples.

The FT-IR data fitting in a thin-film transmission model with the Drude-model dispersion formula (1)-(2) reveals a more detailed picture of the doping effect. Fig. 5 shows how the sample 5 with an implanting dose 10^{14} cm^{-2} deviates from the curve bundle of samples 1-4. A still closer look reveals that the sample 4 refractive index lies consistently 0.1 % below the average value n=3.441 of the samples 1-3 whereas

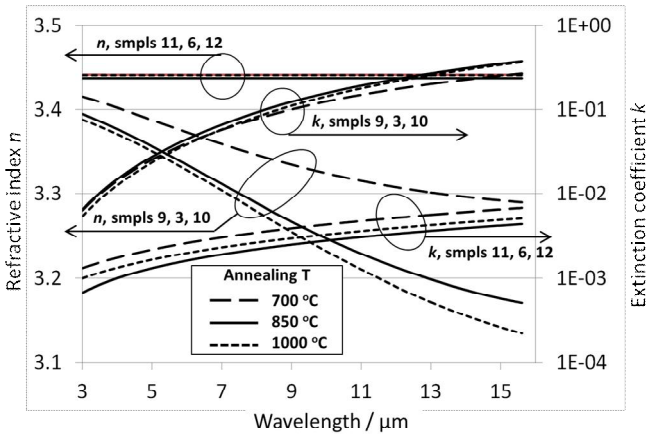

Fig. 6. The temperature effect on n and k. The two sample series represent low and high implanting doses with the annealing-temperature varied. Samples 3 and 6 data is the same as in Fig. 5.

the samples 1-3 mutual scatter is only 0.01 %. On the other hand, the *k* curves of samples 1-4 all lie at 0.001 steps from each other and the mutual order is 1-3-2-4, suggesting the 0.001 is below the noise limit. Since the fitting with the Drude model dispersion formula relates the *n* and *k*, one may suspect whether the apparent consistent separation of sample 4 in the *n* value also remains below the accuracy limit of the present study.

For two of the implanting levels, a series of three samples had the annealing temperature varied: 700°C, 850°C, and 1000°C. Samples 11, 6, and 12 form the lower-dose (2×10^{13} cm^{-2}) series and samples 9, 3, and 10 the higher dose (5×10^{14} cm^{-2}). Fig. 6 summarizes the observation that the low-dose series *n* and *k* do not reveal any dependence on the annealing *T* within the limits of the overall resolution of this study. However, for the higher-dose samples, the refractive index clearly depends on the annealing temperature. Also the extinction coefficient of the 700°C annealed sample deviates from the 850°C and 1000°C counterparts above 10 µm wavelengths.

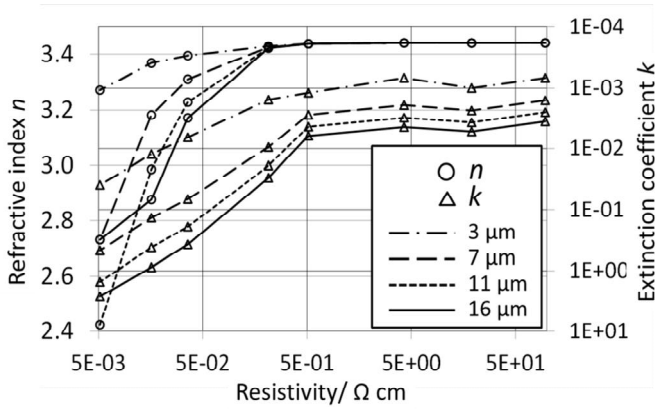

Fig. 7. Plot of the n and k results as a function of the film resistivity. The 8 data-point locations on the resistivity axis from left to right correspond to the samples from8 to 1.

Finally, we plot the optical constants against the resistivity results of each sample. The result that summarizes the work

is shown in Fig. 7. The wavelengths in the plot are selected to represent the limits of the present study (3 μm – 16 μm) and the operation range (7 μm – 11 μm) of the targeted MOEMS application.

IV. Discussion

The *k* curves of the four lightest doped samples in Fig. 5 lie at constant steps of 0.001 and their mutual order from bottom is illogically 1-3-2-4. Since the *n* and *k* values result from a single model-fitting procedure, the *n* curves of the same samples must also be considered randomly scattered around their average. The minimum inaccuracy is 0.005 for *n* and 0.002 for *k*. In Fig. 7, this interpretation implies that the *n* curves should be considered flat and the *k* curves mutual separation noise at the resistivity values above 0.5 Ohm-cm.

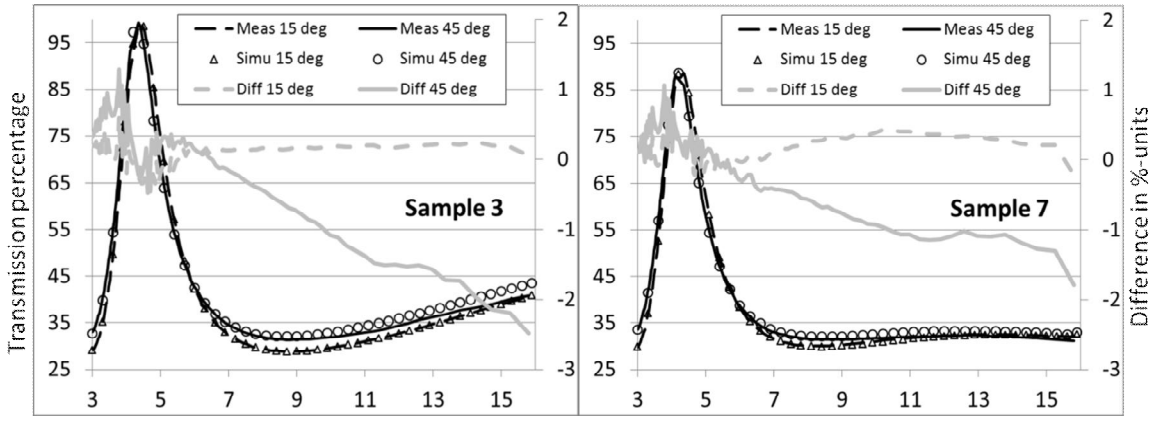

Fig. 8. Simulated transmission curves, the measured data, and their mutual difference. Only the data for 15- and 45-degree incident angles is shown for two selected samples.

In order to evaluate the (*n*,*k*)-result correctness, we estimate the capability of the Drude model to provide the correct dispersion relation for our samples. Fig. 8 presents examples of the measured transmission spectra to be compared with the simulated curves. Simulation model used the *n* and *k* data and the film thickness that resulted from fitting the measurement in the Drude-model dispersion relation. The mutual distance of the curve pairs is a measure of the deviation in the data-fitting procedure. The data fits noisier at the steep features below 7 μm. At longer wavelengths, the simulation result deviates from the measurement with higher incident angle. Generally, the deviation is systematic and thus more a property of the model-fitting mathematics than measurement noise. A systematic measurement error source, like a wavelength-dependent scattering, could also result a similar deviation. A simple failure to correctly determine the incident angle does not seem likely since, offsetting the 45° angle in the model fitting to 44° or 46°, did not improve the result of the comparison.

A word of caution regarding the generality of poly-Si data is justified. Poly-Si films properties are site and recipe dependent. Different LPCVD equipment may produce different grain structure in terms of the size and columnarity with apparently similar deposition recipes.

Finally, let us suggest improvements of the samples and the measurement system for the one planning a similar measurement campaign. The film thickness could have been selected cleverer, if the application does not dictate it. The reliability of the results would benefit from at least two layer thicknesses. Moreover, the poly-Si film thickness could be selected such that the CO_2 absorption peak would occur at a flatter area of the transmission curve – not at a hill top as with our samples. The variable-angle measurement campaign with a FT-IR spectrometer would benefit either from any means to adjust the angle without opening the sample chamber or from an evacuation system to quickly flush out all moisture. A longish dry-air or inert-gas purging may bring along the issues of the FT-IR signal source stability over time.

V. Summary

We resolved the threshold dose of B^+-ion implanting, below which the optical constants remain acceptable for our application in the TIR FPI. Optical data of B^+-doped Si at TIR is not readily available in the literature but comparison with n-type sc-Si [2] indicates that B^+ p-type doped poly-Si shows smaller decrease of the refractive index as a function of the impurity-site concentration.

The result was also presented as a function of the film electrical resistivity. The electrical conduction mechanism of lightly-doped poly-Si was treated as Ohmic and the discussion on a grain-boundary depletion was thus omitted. Comparison of our results against the literature reveals that the electrical resistivity at light doping exceeds the reported [2,18] values for p-type B^+-doped sc-Si whereas, nearly coincide at heavier doping. The trend is in line with a theory [19] of the grain-boundary effects. Our result closely matches to those reported [19] for poly-Si.

ACKNOWLEDGMENT

We are grateful to Mr Noe, of Software Spectra Inc., who provided us with valuable information regarding non-documented batch-processing capabilities of the modelling software TF-Calc. We also wish to acknowledge Ms Häkkinen and Ms Järvi for their precise work in the sample preparation.

REFERENCES

[1] D. F. Edwards, "Silicon (Si)", in *Handbook of Optical Constants of Solids*, vol. 1, E. D. Palik, Ed. Institute for Physical Science and Technology, Univ. of Maryland / Academic Press, London, 1985, pp. 547-569.

[2] S. Kasap, P. Capper, "Chapt. 21: Single-Crystal Silicon" in *Springer Handbook of Electronic and Photonic Materials*, Springer, 2006, pp. 441-480.

[3] T. Abe, T. Kato, "Infrared Reflectivity of N on N^+ Si Wafers", *Jap. J. Appl. Phys.*, vol. 4, 1965, pp. 742-751.

[4] H. H. Wagner, R. R. Schaefer, "Contactless probing of semiconductor dopant profile parameters by ir spectroscopy", *J. Appl. Phys.*, vol. 50, 1979, pp. 2697-2704.

[5] H. Engstrom, "Infrared reflectivity and transmittivity of boron-implanted, laser-annealed silicon", *J. Appl. Phys.*, vol. 51, 1980, 5245-5249.

[6] H. Piller, "Silicon (Amorphous)", in *Handbook of Optical Constants of Solids*, vol. 1, E. D. Palik, Ed. Institute for Physical Science and Technology, Univ. of Maryland / Academic Press, London, 1985, pp. 571-586.

[7] S. He, A. B. Sproul, "Optical properties of evaporated poly-Si thin-films on glass", *Thin Solid Films*, vol. 519, 2010, pp. 351-356.

[8] H. Chen, W. Z. Shen, "Optical characterization of boron-doped nanocrystalline Si:H thin films", *Surf. Coat. Technol.* vol. 198, 2005, pp. 98-103.

[9] Y. Laghla, E. Scheid, "Optical study of undoped, B or P-doped polysilicon", *Thin Solid Films*, vol. 306, 1997, pp. 67-73.

[10] Y. Laghla, E. Scheid, H. Vergnes, J.P. Couderc, "Electronic properties and microstructure of undoped, and B- or P-doped polysilicon deposited by LPCVD", *Sol. Energy Mater. Sol. Cells*, vol. 48, 1997, pp. 303-314.

[11] A. F. Turner, B. W. Baumeister, "Multilayer Mirrors with High Reflectance Over an Extended Spectral Region", *Appl. Opt.*, vol. 5, 1966, pp. 69-76.

[12] J. M. Vaughan, *The Fabry-Perot Interferometer: History, Theory, Practice and Applications*,Taylor & Francis Group, New York / London,1989.

[13] M. Tuohiniemi, M. Blomberg, "Surface-micromachined silicon air-gap Bragg reflector for thermal infrared", *J. Micromech. Microeng.*, vol. 21 (2011) 075014, 7pp.

[14] M. Tuohiniemi, M. Blomberg, A. Akujärvi, J. Antila, H. Saari,"Optical transmission performance of a surface-micromachined Fabry–Perot interferometer for thermal infrared", *J. Micromech. Microeng.* vol. 22, 2012, 115004, 7pp.

[15] H. G. Tompkins, W.A. McGahan, *Spectroscopic Ellipsometry and Reflectometry – A User's Guide*, John Wiley & Sons, Inc., 1999, pp.35-39.

[16] M. Schubert, *Infrared Ellipsometry on Semiconductor Layer Structures*, Springer-Verlag, Berlin Heidelberg, 2004, pp. 1-27.

[17] N. W. Ashcroft, N.D. Mermin, *Solid State Physics*, Brooks/Cole – Thomson Learning, 1976, pp.2-27.

[18] W. R. Thurber, R. L. Mattis, Y. M. Liu, J. J. Filliben, "Resistivity-Dopant Density Relationship for Boron-Doped Silicon", *J. Electrochem. Soc.*, vol. 127, 1980, pp. 2291-2294.

[19] N. C.-C. Lu, L. Gerzberg, C.-Y. Lu, J. D. Meindl, "Modeling and Optimization of Monolithic Polycrystalline Silicon Resistors", *IEEE Trans. Electron Devices*, vol. 28, 1981, pp. 818-830.